Journal of ELECTRONIC MATERIALS, Vol. 47, No. 1, 2018
DOI: 10.1007/s11664-017-5829-6

Comparison of NO_2 Gas-Sensing Properties of Three Different ZnO Nanostructures Synthesized by On-Chip Low-Temperature Hydrothermal Growth

MINGZHI JIAO,[1] NGUYEN VAN DUY,[2] DO DANG TRUNG,[2] NGUYEN DUC HOA,[2] NGUYEN VAN HIEU,[2] KLAS HJORT,[1] and HUGO NGUYEN[1,3]

1.—Department of Engineering Sciences, Uppsala University, Lägerhyddsvägen 1, 751 21 Uppsala, Sweden. 2.—International Training Institute for Materials Science, Hanoi University of Science and Technology, No 1 Dai Co Viet, Hanoi, Vietnam. 3.—e-mail: Hugo.nguyen@angstrom.uu.se

Three different ZnO nanostructures, dense nanorods, dense nanowires, and sparse nanowires, were synthesized between Pt electrodes by on-chip hydrothermal growth at 90°C and below. The three nanostructures were characterized by scanning electron microscopy and x-ray diffraction to identify their morphologies and crystal structures. The three ZnO nanostructures were confirmed to have the same crystal type, but their dimensions and densities differed. The NO_2 gas-sensing performance of the three ZnO nanostructures was investigated at different operation temperatures. ZnO nanorods had the lowest response to NO_2 along with the longest response/recovery time, whereas sparse ZnO nanowires had the highest response to NO_2 and the shortest response/recovery time. Sparse ZnO nanowires also performed best at 300°C and still work well and fast at 200°C. The current–voltage curves of the three ZnO nanostructures were obtained at various temperatures, and the results clearly showed that sparse ZnO nanowires did not have the linear characteristics of the others. Analysis of this phenomenon in connection with the highly sensitive behavior of sparse ZnO nanowires is also presented.

Key words: ZnO nanostructures, NO_2, gas sensor, hydrothermal, on-chip

INTRODUCTION

NO_2 is an air pollutant harmful to human health. The presence of this pollutant is severely increasing, especially in the urban environment, due to the increase of automobiles. Therefore, highly sensitive NO_2 gas sensors are useful for monitoring NO_2 in urban areas. ZnO is an *n*-type semiconductor and has inherent defects, such as oxygen vacancy,[1] therefore possessing high NO_2 sensitivity.[2] ZnO nanostructures can easily be obtained by liquid or gas phase growth. In addition, ZnO nanostructures can be modified to increase the sensitivity and selectivity.[3] In most works, ZnO nanostructures were first grown, harvested, and then placed between electrodes to be used as a gas-sensing material. For example, ZnO nanorods obtained at 110°C by ultrasonic spray pyrolysis have a response, defined as R_{gas}/R_{air}, of 200–5 ppm NO_2 at 250°C.[4] Tube-like ZnO solvothermal nanostructures synthesized at 150°C have a response of approximately 350 to 11.5 ppm NO_2 at 190°C.[5] Pencil-like ZnO nanorods, obtained via cetrimonium bromide (CTAB)-assisted hydrothermal process at 90°C, have a highest response of 206 to 40 ppm NO_2 at 400°C.[6] Many other similar studies were performed using ZnO one-dimensional (1D) nanostructures for NO_2 sensing. The summary is presented in Table I.

(Received March 22, 2017; accepted September 27, 2017; published online October 23, 2017)

Table I. Recent works on ZnO nanostructures made by a wet route for NO_2 sensing

Morphologies	Synthesis method/ temp (°C)	Diameter (nm)	Response/ ppm	Sensitivity	Working temp (°C)
Nanorods with nanovoids[7]	Hydrothermal/160	23	51/10	5.1	250
Nanoprism[8]	Continuous hydrothermal pilot plant/400	32	128/10	12.8	350
Needle-like nanorods[9]	Reverse micro-emulsion/120	52	624/40	15.6	120
Nanorods[10]	Solvothermal/120	20–25	44.2/50	0.88	300
Nanorod arrays[11]	Reflux/95	39	32/100	0.32	175

ZnO nanostructures can also be fabricated using a dry process and then placed between electrodes as a NO_2 sensor. For example, ZnO tetrapods synthesized at 700°C have a response of 20 to 20 ppm NO_2 at 300°C.[7] Branched ZnO nanowires synthesized by two-step thermal evaporation processes at 950°C have a response of 2.06 to 5 ppm NO_2 at 300°C.[8] Crystalline ZnO nanocombs synthesized by chemical vapor deposition (CVD) at 700°C have a response of more than 100 to 5 ppm NO_2 at 200°C.[9] The CVD method can produce many different ZnO nanostructures, but the high temperature limits the opportunity for gas sensing on flexible substrates. For the non-on-chip growth method, optimized ZnO nanostructures can be very sensitive to NO_2 but the transfer process causes the sensor to have low reproducibility due to poor adhesion and random placement of nanostructures between the electrodes. Notably, the performance of a ZnO nanorod gas sensor also depends on the position of the electrodes, with the bottom electrode design being better than the top one.[10] The bottom electrodes are best fabricated first and then the ZnO nanostructures are grown between the electrodes on-chip for gas measurement.[11–13] Recently, ZnO nanowires have been selectively grown between Pt electrodes by CVD on discrete Au islands and used for gas sensing of NO_2 and ethanol.[14] Recently, we successfully grew ZnO nanorods via the hydrothermal method on-chip at 85°C and found that the nanorods have good sensitivity and selectivity to NO_2.[15] However, the response of the ZnO nanorods to NO_2 is not as high as reported for other ZnO nanostructures. As shown in previous work, the morphology of ZnO can significantly influence gas sensing to NO_2.[16–18] Here, we grow different ZnO nanostructures on-chip by a low-temperature hydrothermal method and investigate the influence of morphology on NO_2 gas sensing.

EXPERIMENTAL

ZnO Nanostructures Preparation

The steps of manufacturing of the sensor device are shown in the top panels of Fig. 1, where the sensor electrodes were patterned by lithography, vapor deposition, and lift-off of 100 nm of Pt on 10-nm Cr layers on a glass substrate. Seed islands of Zn with a thickness of 15 nm on a 10-nm silicon layer were deposited on and between the electrodes using the same techniques (three bottom panels on the left). ZnO nanostructures were grown from the seed islands with a similar hydrothermal method as presented in Ref. 15 (last bottom panel on the right). Note that the bottom panels from left to right show a fabricated sensor chip with dimensions of 4×4 mm and close-ups of its center part. The three different ZnO nanostructures, i.e., dense nanorods, dense nanowires, and sparse nanowires, hereafter abbreviated as ZnO-NR, ZnO-NW_d, and ZnO-NW_s, respectively, were synthesized in a precursor solution of equimolar hexametylenetetramine (HMTA) and $Zn(NO_3)_2$ with the following detailed conditions.

(a) Synthesis of ZnO-NR

ZnO-NR were grown at 85°C for 16 h in a convection oven using a mixture of 50 mL 0.01 M $Zn(NO_3)_2$ and 50 mL 0.01 M HMTA. After growth, the chips were taken out and rinsed in DI-water three times and dried at 60°C for 12 h.

(b) Synthesis of ZnO-NW_d

ZnO-NW_d were grown in a water bath. The precursor concentration for ZnO-NW_d was 0.0025 M after mixing of $Zn(NO_3)_2$ and HMTA. The water bath was first kept at 70°C for 5 h and then increased to 90°C and kept at this temperature for 24 h.

(c) Synthesis of ZnO-NW_s

ZnO-NW_s were also grown in a water bath, but in two steps. The first step used a 0.001-M equimolar mixture of $Zn(NO)_2$ and HMTA. The bath was kept at 60°C for 1 h and then increased to 70°C and kept there for 3 h and finally at 90°C for 24 h. Afterwards, the glass chips were taken out and rinsed in DI-water. For the second step, a fresh precursor solution with a concentration of 0.0005 M after mixing of $Zn(NO_3)_2$ and HMTA was used. The water bath was kept at 70°C for 1 h and then increased to 90°C and kept at this temperature for 24 h. After growth, the chips were taken out and rinsed in DI-water three times and dried at 60°C for 12 h.

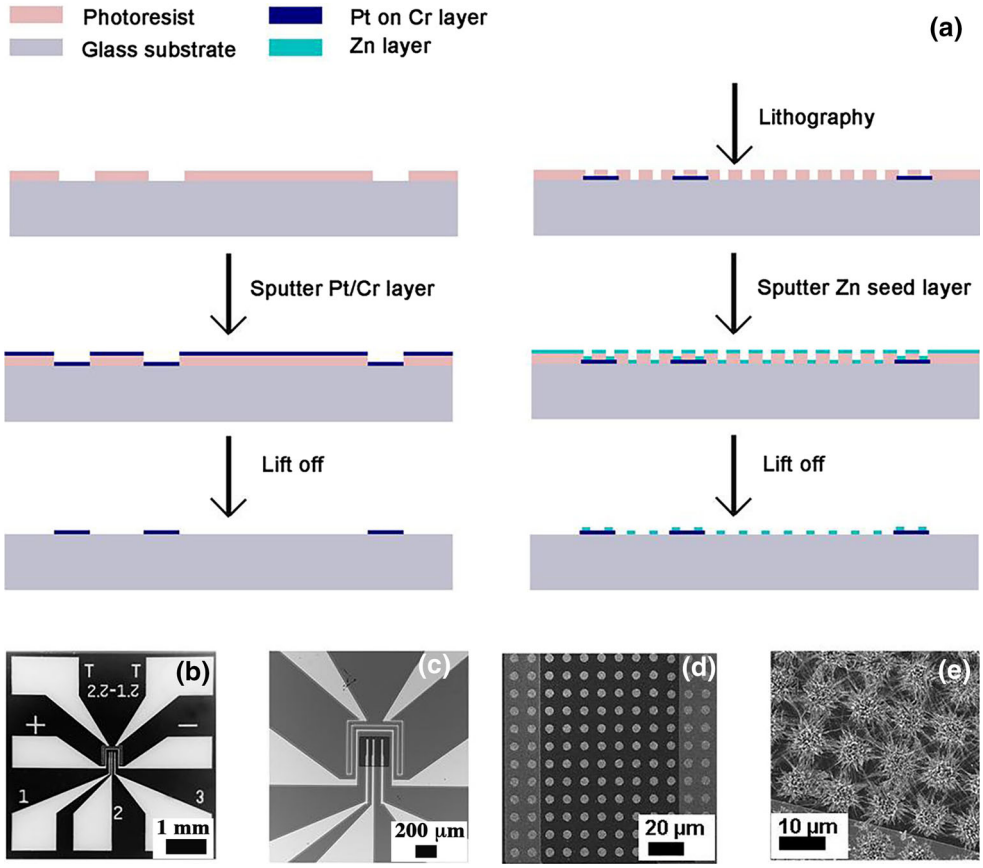

Fig. 1. Process flow for device fabrication (a) and SEM images of as-fabricated device with different magnification (b–e).

Material Characterization

The morphologies of the three ZnO nanostructures were investigated by using field emission scanning electron microscopy (FESEM; JEOL JSM-7600F). Transmission electron microscopy (TEM) images were performed by a JEOL JEM-2100F. The crystal structures of the ZnO nanostructures were investigated by grazing-incidence x-ray diffraction (Parallel Beam Geometry with x-ray mirrors; SIEMENS D5000, Germany) using CuKα radiation (λ = 1.5406 Å) in the range of 20°–80°. The incidence angle was set at 0.3° during the measurements.

Gas Measurement

The sensors were annealed at 650°C for 3 h before gas measurement to ensure the uniformity and stability of the devices. They were then tested using a standard flow rate of 400 sccm for both dry air and mixed gas. The standard gas, i.e., 1000 ppm NO_2 balanced with N_2, was mixed with dry air by a series of mass flow controllers to obtain different lower concentrations, namely 2.5 ppm, 5 ppm, 10 ppm, and 25 ppm.[14] During the sensing measurements, a Keithley multimeter (model 2700) was used to automatically acquire the resistance data. The full response/recovery time was set before the measurement. Before the four-cycle measurement, a test run with a concentration of 2.5 ppm was performed. Then, the full response/recovery time is set according to the data from 2.5 ppm in the measurement program. The program will switch the measured gas flow controller on and off according to this setting. In the presentation of the results, the response time for the sensor is instead the time taken to obtain 90% of the total response for 2.5 ppm NO_2 from the time point of introducing NO_2 gas into the measurement chamber. Similarly, the recovery time is the time taken to recover 90% of the total response from the time point of switching off the 2.5 ppm NO_2 gas.

The sensor response to the test gas is defined as $R = R_{gas}/R_{air}$, where R_{gas} is the sensor resistance under NO_2 gas exposure and R_{air} is the resistance in the dry air, i.e., in the absence of the test gas. The influence of humidity is small for our measurement (temperature higher than 200°C).

RESULTS AND DISCUSSION

Morphologies of the three different ZnO nanostructures were examined by SEM. As seen in Fig. 2a, ZnO nanorods (ZnO-NR) form junctions between one another. The diameter of the nanorods

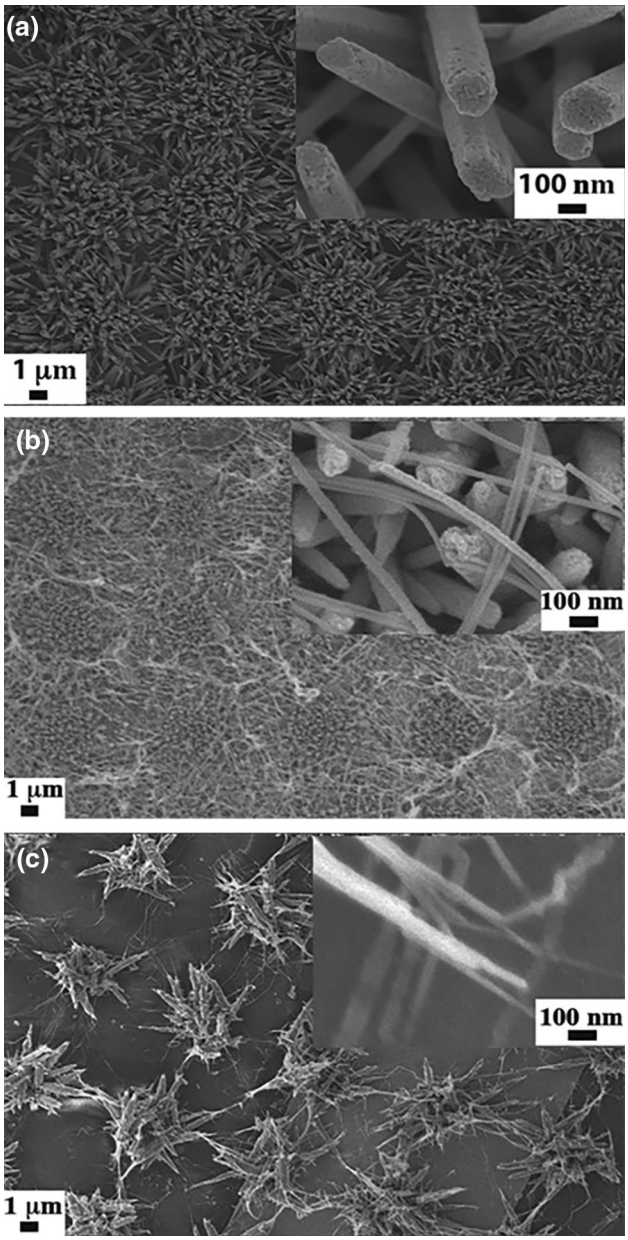

Fig. 2. SEM images of the three ZnO nanostructures: (a) ZnO-NR, (b) ZnO-NW_d, and (c) ZnO-NW_s. The insets are magnifications of the respective images.

ranges from 150 nm to 200 nm. Figure 2b shows that very dense ZnO secondary nanowires (ZnO-NW_d) were grown from the primary ZnO nanorods and are also connected to one another. The secondary nanowires have a diameter of approximately 25–50 nm. Figure 2c shows that sparse ZnO secondary nanowires (ZnO-NW_s) were also grown from primary nanorods and then connected to one another, but the density was much lower than that in Fig. 2b. The diameter of these nanowires is less than 25 nm. This value is comparable to the Debye length of ZnO, and thus expected to show high gas sensitivity.

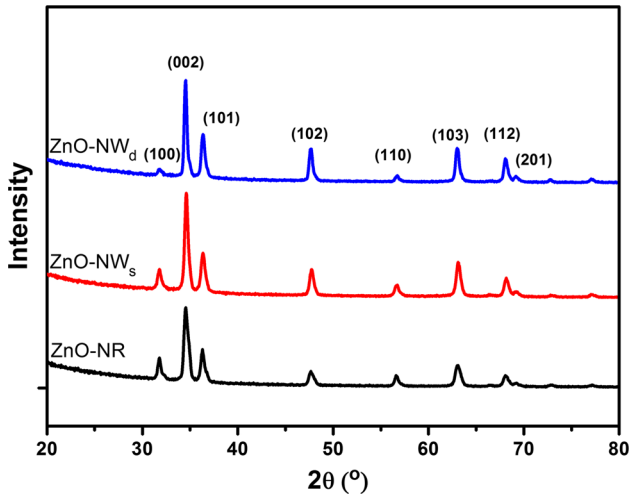

Fig. 3. GI-XRD of the three ZnO nanostructures; incidence angle at 0.3°.

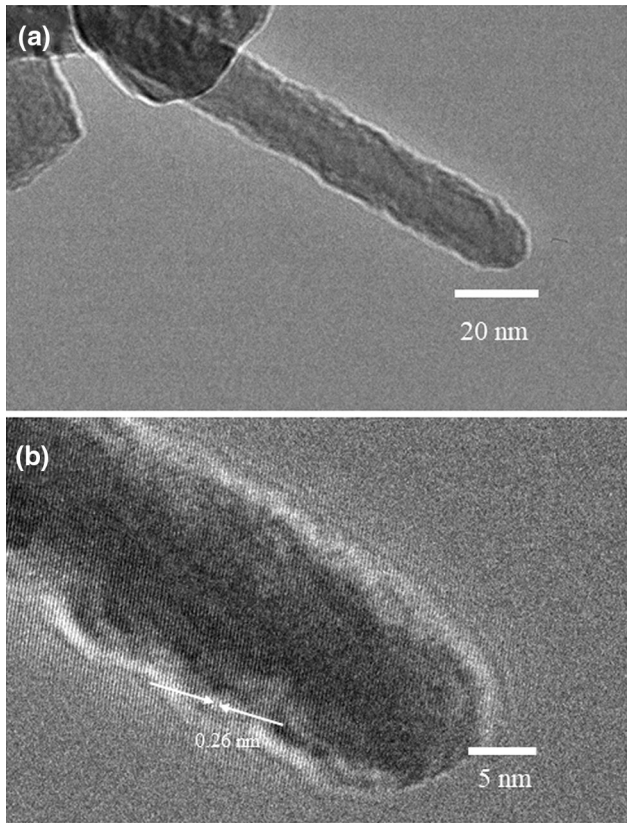

Fig. 4. TEM images of ZnO-NWs: (a) TEM; (b) HRTEM images.

Figure 3 shows crystal types of the three ZnO samples examined by grazing-incidence XRD. All three samples have similar peak positions and intensities. They all have hexagonal crystal structures (Reference code 00-036-1451). From the XRD data, the average crystal size of the ZnO nanostructures can be estimated by the Scherrer equation using (002) peaks to be about: 29.2 nm for ZnO-

NW_d, 23.5 nm for ZnO-NW_s, 17.5 nm for ZnO-NR. It is somehow questionable that the average crystal size of ZnO-NR is much smaller than their diameter estimated by SEM images, while other reports have revealed the single crystallinity of ZnO nanorod grown by the HMTA pathway.[19] It is worth noting that the crystal size calculation by the Scherrer equation needs to be calibrated by a known sample or TEM characterization. Anyway, XRD data confirm the single phase of ZnO in three samples.

To further study the morphology and crystallinity of the hydrothermal synthesized ZnO, we checked the TEM images of ZnO-NW_s, and the data are shown in Fig. 4. As we can see, the ZnO-NW_s has a diameter of about 20 nm with a rough surface (Fig. 4a). The HRTEM image (Fig. 4b) reveals the single crystal nature of the ZnO-NW_s, where clear lattice fringes are presented. The gap between the lattice fringes is 0.26 nm, corresponding to the interspace of (002) planes. This result is consistent with the observation by XRD, where the (002) peak is the strongest, suggesting its preferred growth direction.

Next, dynamic NO_2 sensing curves of all the three ZnO samples are presented (Fig. 5). The response/recovery time decreases as the working temperature increases due to the adsorption and desorption process of the gas species that accelerates at higher temperature. Both ZnO-NW_d and ZnO-NW_s samples have much shorter response/recovery times than the ZnO-NR sample, especially at 400°C. They can also work better at lower temperatures than the ZnO-NR. Notably, the ZnO-NW_s still respond and recover quickly even at 200°C, while ZnO-NW_d already responds and recovers very slowly at 250°C. For ZnO-NR, it was so slow that it was not worth measuring at temperatures below 350°C. Despite the diameter difference, the base resistance of ZnO-NR and ZnO-NW_d is of the same order, while ZnO-NW_s has a base resistance two orders higher than the other two. This means that the density and diameter of the ZnO nanostructures significantly influence the device properties. The different resistances of different nanostructures to NO_2 gas are mainly due to the different diameters of the samples. As we know, the surface depletion layer will influence the whole nanorod when the diameter of the nanorod is equal to or smaller than the width of surface depletion layer. Different samples also have different base resistances. For example, the base resistance of ZnO nanorod at 350°C is 1.5×10^4 Ω while that of ZnO-NW_s is 1.2×10^6 Ω. The concentration–response curves of all three samples show a linear tendency within the concentration range.

Table II summarizes the numerical values of parameters of the three samples. The optimal work temperature of ZnO-NW_s decreases to 300°C. The response/recovery time of this sample significantly decreases compared with that of the other two. Its response to 2.5 ppm NO_2 at this temperature is still as high as 14.92. This means that ZnO-NW_s can be used as a fast and sensitive NO_2 sensor. Sensitivity, defined as response divided by concentration, can be used to compare our sample with the others, since test gas concentrations are usually different in different works. As presented in Table I, most 1D ZnO nanostructures were synthesized at temperatures higher than 100°C. ZnO-NW_s has a sensitivity value of 4.71 to 10 ppm NO_2, which is comparable to the sensitivity of ZnO nanorods with nanovoids synthesized at 160°C to the same concentration of NO_2. Needle-like nanorods have sensitivity value of 15.6, which is higher than our ZnO-NW_s. However, the sample was synthesized at 120°C. Our sample was synthesized at a temperature lower than 100°C and was much easier to scale-up. The highest sensitivity of nanorod arrays synthesized at 95°C is less than 1 per ppm, whereas the highest sensitivity of our ZnO-NW_s is 6 per ppm as calculated from our measurements.

Figure 6 shows that the ZnO-NW_s sample has a higher response to 2.5 ppm NO_2 compared with the other two samples at all measured temperatures. The columns for the ZnO-NR sample at 250°C and 300°C are missing in this figure due to its very slow response which was not worth measuring. At 300°C, the response of ZnO-NW_s is three times higher than that of ZnO-NW_d. This figure also shows that the responses of the ZnO-NR and ZnO-NW_d samples are almost unchanged with their operation temperatures, whereas the response of the ZnO-NW_s sample increases dramatically with a decrease of the operation temperature, and its highest response occurs at 300°C. At temperatures lower than 300°C, the response of ZnO-NW_s decreases.

To investigate the better sensing performance of ZnO-NW_s at low temperatures, a series of *I–V* measurements of all the three samples were performed in ambient air at temperatures of 250°C, 350°C, and 450°C (Fig. 7). The applied voltage within ± 10 V was chosen because it covers the sensor operation voltage of ± 5 V to a large extent. *I–V* curves in Fig. 7a and b show that ZnO-NR and ZnO-NW_d samples have an ohmic behavior, i.e., a linear characteristic. The curves for each temperature have very similar trends and almost overlap one another, at least for the selected operation voltages, showing that the resistance of the samples does not change very much with temperature (Fig. 7d). The *I–V* curves of ZnO-NW_s, on the other hand, are very different from the other two (Fig. 7c). First, the three curves do not pass through the zero point. This is because much more photo current exists in this sample than in the other two due to the fact that these measurements were performed in daylight. Second, ZnO-NW_s has an ohmic behavior at low temperature, but a non-ohmic behavior as temperature increases. The non-linear behavior of ZnO can be influenced by barrier height.[19] Many more oxygen ions will be adsorbed onto the surface of the ZnO-NW_s at 450°C so that the width of the surface depletion layer will increase. The contact

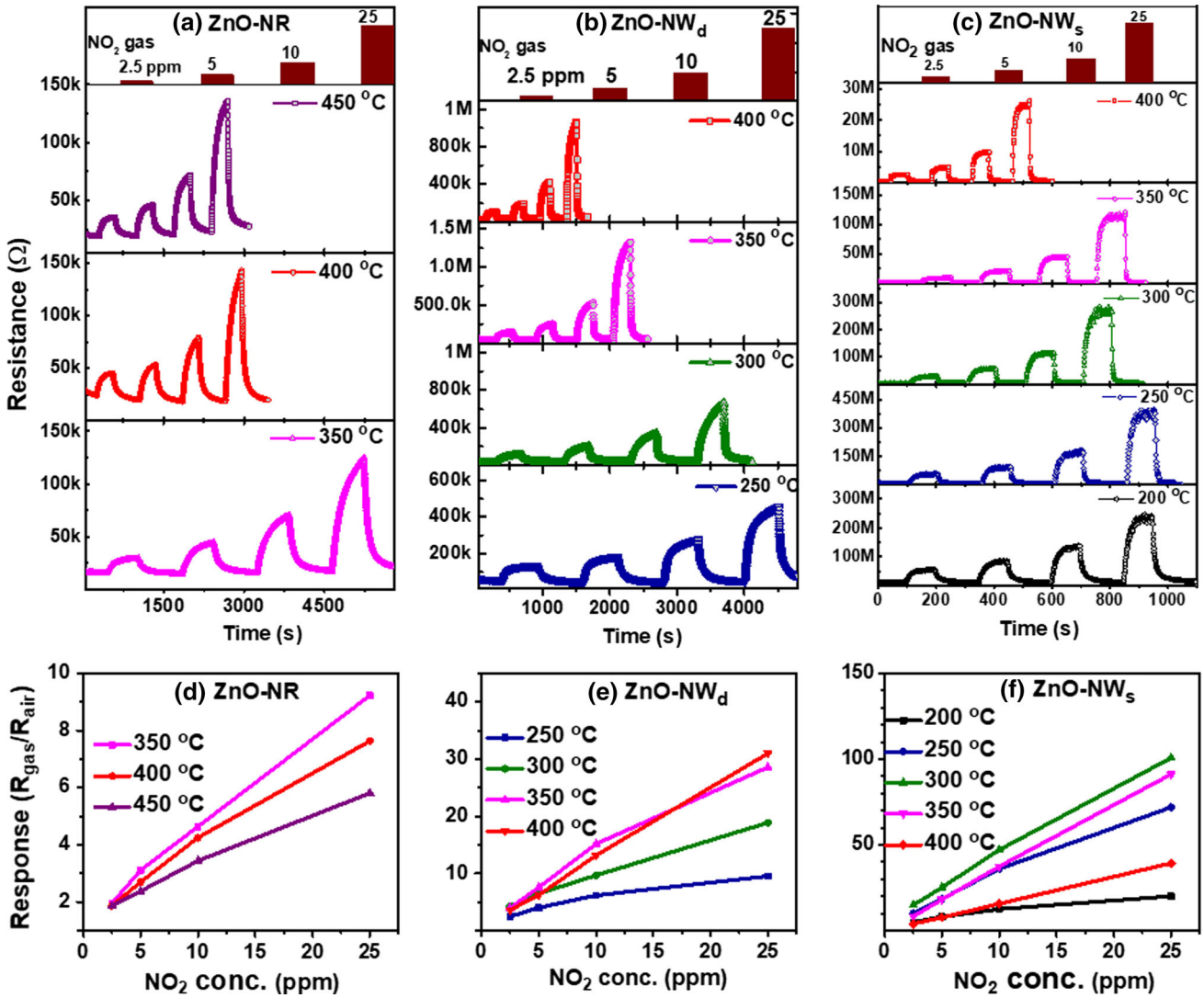

Fig. 5. Dynamic gas sensing of three ZnO samples and comparison of response at different temperatures for each sample. (a–c) transient response and (d–f) response as a function of gas concentration.

Table II. Comparison of best sensing performance of the three ZnO samples to 2.5 ppm NO_2

Sample	Optimum work temperature (°C)	Response time (s)	Recovery time (s)	Response
ZnO-NR	350	226	264	1.96
ZnO-NWd	350	113	169	4.1
ZnO-NWs	300	52	101	14.92

barrier of ZnO-NW_s is very high at 450°C. So the sample shows a non-ohmic *I–V* behavior. The resistances of ZnO-NR and ZnO-NW_d extracted from the *I–V* curves at 5 V decrease with the increase of temperature according to the semiconductor behavior, whereas the resistance increases for ZnO-NW_s (Fig. 7c). Thus, the good sensing performance of ZnO-NW_s at low temperature should be related to this phenomenon.

The gas-sensing mechanism of the nanostructures is based mainly on their surface interaction with gases in the surrounding environment. The surface of the ZnO nanostructure is normally terminated by oxygen species in the air.[20,21] The type of adsorbed oxygen species depends on temperature,[18,22] as described in four steps below.

$$O_2\,(g) \rightarrow O_2\,(\text{Physical adsorption}) \qquad (1)$$

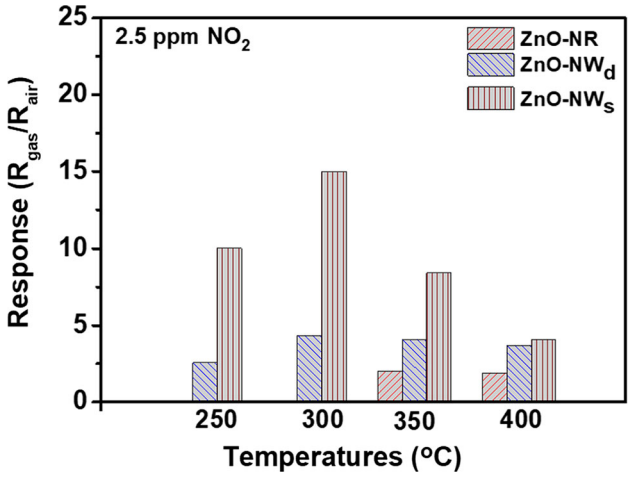

Fig. 6. Comparison of sensing response of the three ZnO samples to 2.5 ppm NO_2 at temperatures of 250°C, 300°C, 400°C, and 450°C.

$$e^- + O_2 \rightarrow O_2^- \text{ (Ionic adsorption; } < 100^\circ C) \quad (2)$$

$$2e^- + O_2^- \rightarrow 2O^- \text{ (Ionic adsorption; } 100^\circ C \text{ to } 300^\circ C) \quad (3)$$

$$e^- + O^- \rightarrow O^{2-} \text{ (Ionic adsorption; } > 300^\circ C) \quad (4)$$

At low temperatures, oxygen is only physically adsorbed to the surface of ZnO, without forming any ionic bond. As the temperature increases, physically adsorbed oxygen will take more electrons from the surface of ZnO and form charged oxygen species (steps 2–4), resulting in higher resistance of the depletion layer at the surface of the sensing material.

As discussed in Ref. 23, the conductivity of the gas-sensing material depends on the bulk and the depletion layer. Thus, as the temperature increases, the resistance of the ZnO material on all three

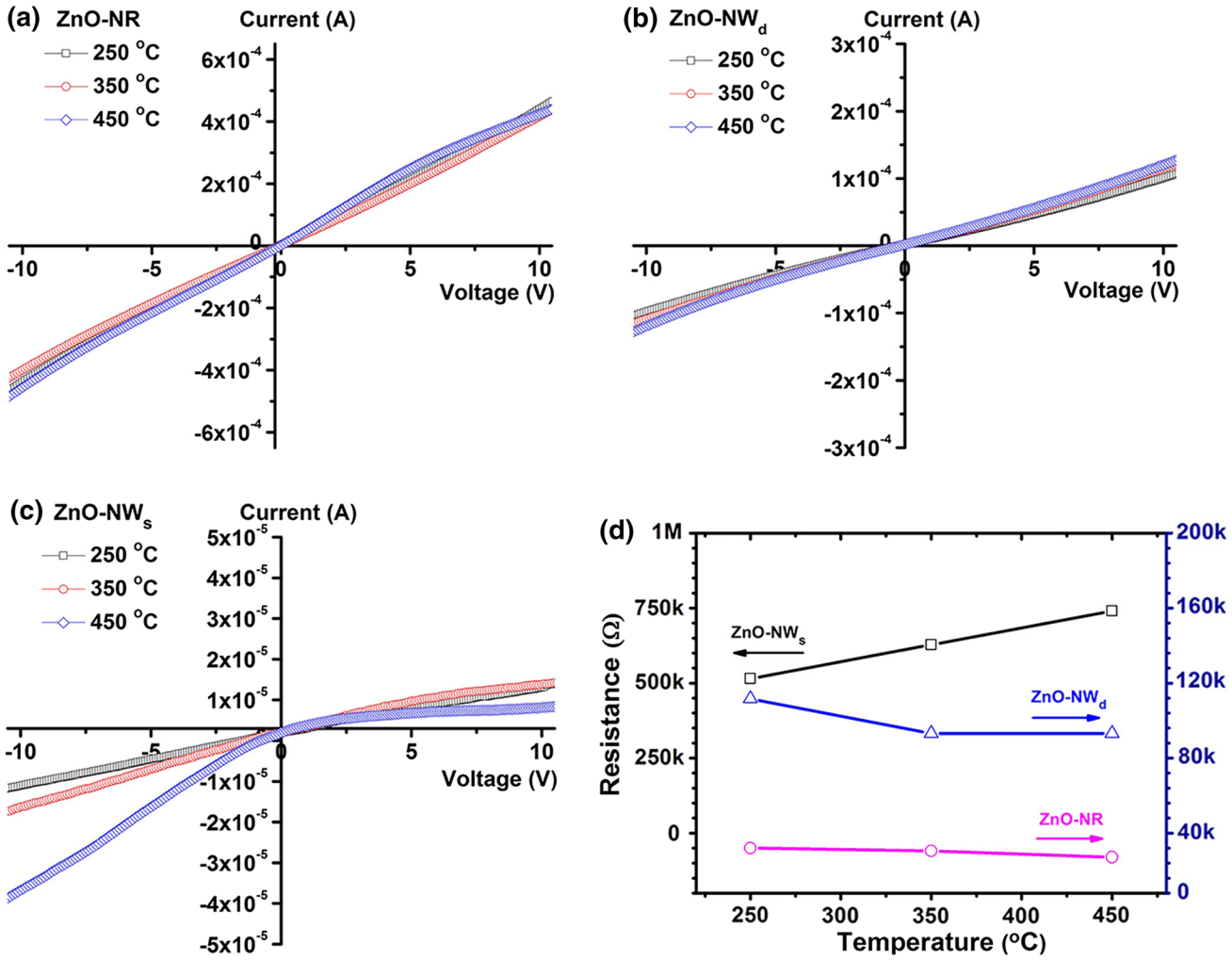

Fig. 7. *I–V* curves of the three ZnO nanostructures at different temperatures (a–c); resistance extracted from *I–V* curves of each sample at different temperatures for the applied voltage of 5 V (d).

samples increases due to the higher activity of oxygen from the air, but decreases due to the behavior of the semiconducting material. For ZnO-NR, the diameter of the nanorods is much larger than the Debye length, which is approximately 20 nm,[24] so that the change of the depletion layer only slightly influences the conductivity of this sample. Therefore, the measured resistance (i.e., dV/dI) (Fig. 7d) is almost unchanged under different temperatures. The small decrease of the resistance might be attributed to the semiconductor behavior of the ZnO material. For the ZnO-NW_d samples, the diameter of the nanowires is approximately 2–5 times greater than that of the Debye length. In other words, the radius is approximately similar to or 2.5 times greater than the Debye length. Thus, the influence of the surface depletion on the conductivity is considerable.[25] However, the dense nanowires constitute the numerous parallel connections between the sensor electrodes, so that the influence of surface depletion is minimized. Therefore, the change of resistance versus temperature for this sample resembles that of the ZnO-NR sample (Fig. 7d). For the ZnO-NW_s sample, on the other hand, very few nanowires are found, and their diameter is even smaller than that on the ZnO-NW_d sample. Therefore, the surface depletion layer considerably influences the resistance of ZnO and dominates the semiconductor behavior of these nanowires as can also be seen in Fig. 7d. The contribution of the junctions between the nanorods and between the nanowires on all three samples to their resistance under the influence of the depletion mechanism is important and should be subjected to the same explanation as the bulk material of the nanorods and nanowires.

A quantitative analysis can be performed from the view of electrical measurement. Given that the resistance of a gas sensor is measured between two probes on Pt electrodes, the total resistance of the sensor is

$$R_{\mathrm{tot}} = R_{\mathrm{pr}} + R_{\mathrm{pr/Pt}} + R_{\mathrm{Pt}} + R_{\mathrm{Pt/ZnO}} + R_{\mathrm{ZnO}},$$

where R_{pr} is the resistance of the probes, $R_{\mathrm{pr/Pt}}$ is the contact resistance between the probe and Pt electrodes, R_{Pt} is the resistance of Pt, $R_{\mathrm{Pt/ZnO}}$ is the contact resistance between Pt and ZnO nanostructures, R_{ZnO} is the resistance of ZnO nanostructures. Given that R_{ZnO} and its change versus temperature is in the range of kΩ and MΩ, the first three are much smaller resistances (with ohmic behavior) and can be omitted. $R_{\mathrm{Pt/ZnO}}$, as seen from the I–V sweeping from – 10 V to + 10 V in Fig. 7, does not possess Schottky contact behavior and is also small compared with R_{ZnO}. Therefore, it can also be omitted in the resistance analysis.

CONCLUSION

We have successfully synthesized three different types of ZnO nanostructures on-chip by a low-temperature hydrothermal method. Nanorods of the first type have larger diameters compared with the nanowires of the two other types. The NWs of the second type were dense, and that of the third type very sparse. Their average diameters are slightly different. A smaller diameter has been shown to be better for NO_2 sensing. A lower density of nanowires gives a higher response to NO_2 and shorter response/recovery times than a higher nanowire density. The low-density nanowires can also function at a lower temperature than the other two. The mechanism of the gas-sensing response is explained by a surface depletion model. A high response of sparse ZnO nanowires is based on the large contribution of the surface depletion layer to the resistance of the material. These sparse ZnO nanowires work best at 300°C.

ACKNOWLEDGEMENTS

The authors thank the China Scholarship Council (CSC) for Grant No. 201206340092 and Uppsala University for financial support of Mingzhi Jiao's Ph.D. studies, and the Vietnam National Foundation for Science and Technology Development (NAFOSTED) for Grant No. 103.02-2015.15.

REFERENCES

1. M.D. Mccluskey and S.J. Jokela, *J. Appl. Phys.* 106, 71101 (2009).
2. M. Ahn, K. Park, J. Heo, J. Park, D. Kim, K.J. Choi, J. Lee, S. Hong, M. Ahn, K. Park, J. Heo, J. Park, D. Kim, K.J. Choi, and J. Lee, *Appl. Phys. Lett.* 93, 263103 (2008).
3. R. Kumar, G. Kumar, and A. Umar, *Nano-Micro Lett.* 7, 97 (2015).
4. F.-T. Liu, S.-F. Gao, S.-K. Pei, S.-C. Tseng, and C.-H.J. Liu, *J. Taiwan Inst. Chem. Eng.* 40, 528 (2009).
5. M. Chen, Z. Wang, D. Han, F. Gu, and G. Guo, *Sens. Actuators B* 157, 565 (2011).
6. B. Shouli, L. Xin, L. Dianqing, C. Song, L. Ruixian, and C. Aifan, *Sens. Actuators B* 153, 110 (2011).
7. D. Calestani, M. Zha, R. Mosca, A. Zappettini, M.C. Carotta, V. Di Natale, and L. Zanotti, *Sens. Actuators B* 144, 472 (2010).
8. S. An, S. Park, H. Ko, C. Jin, W. In, and C. Lee, *Thin Solid Films* 547, 241 (2013).
9. X. Pan, X. Liu, A. Bermak, and Z. Fan, *ACS Nano* 7, 9318 (2013).
10. S. Öztürk, N. Kılınç, and Z. Ziya, *J. Alloys Compd.* 581, 196 (2013).
11. A.Z. Sadek, S. Member, S. Choopun, W. Wlodarski, S.J. Ippolito, and K. Kalantar-zadeh, *IEEE Sens. J.* 7, 919 (2007).
12. E. Oh, H. Choi, S. Jung, S. Cho, J. Chang, K. Lee, S. Kang, J. Kim, J. Yun, and S. Jeong, *Sens. Actuators B* 141, 239 (2009).
13. M.-W.W. Ahn, K.-S.S. Park, J.-H.H. Heo, D.-W.W. Kim, K.J.J. Choi, and J.-G.G. Park, *Sens. Actuators B* 138, 168 (2009).
14. H. Nguyen, C. Thi, N. Duc, N. The, and N. Van Duy, *Sens. Actuators B* 193, 888 (2014).

15. M. Jiao, N. Viet, N. Van Duy, and N. Duc, *Mater. Lett.* 169, 231 (2016).
16. M.C. Carotta, A. Cervi, V. di Natale, S. Gherardi, A. Giberti, V. Guidi, D. Puzzovio, B. Vendemiati, G. Martinelli, M. Sacerdoti, D. Calestani, A. Zappettini, M. Zha, and L. Zanotti, *Sens. Actuators B* 137, 164 (2009).
17. C.T. Quy, C.M. Hung, N. Van Duy, N.D. Hoa, M. Jiao, and H. Nguyen, *J. Electron. Mater.* 46, 3406 (2017).
18. Y. Şahin, S. Öztürk, N. Kılınç, A. Kösemen, M. Erkovan, and Z.Z. Öztürk, *Appl. Surf. Sci.* 303, 90 (2014).
19. R. Ahmad, N. Tripathy, and Y.-B. Hahn, *Biosens. Bioelectron.* 45, 281 (2013).
20. H. Chon, *J. Catal.* 14, 257 (1969).
21. S. Fujitsu, K. Koumoto, H. Yanagida, Y. Watanabe, and H. Kawazoe, *Jpn. J. Appl. Phys.* 38, 1534 (1999).
22. J. Ding, J. Zhu, P. Yao, J. Li, H. Bi, and X. Wang, *Ind. Eng. Chem. Res.* 54, 8947 (2015).
23. N. Barsan and U. Weimar, *J. Electroceram.* 7, 143 (2001).
24. A. Katoch, S.-W. Choi, G.-J. Sun, and S.S. Kim, *J. Mater. Chem. A* 1, 13588 (2013).
25. C.C. Li, Z.F. Du, L.M. Li, H.C. Yu, Q. Wan, and T.H. Wang, *Appl. Phys. Lett.* 91, 32101 (2007).